DISTRIBUTION STATEMENT A. Approved for public release; distribution is unlimited.

Satellite SAR Exploitation and Imaging and Measurement of Oceanic Phenomena

Hans C. Graber
CSTARS - University of Miami
11811 SW 168th Street
Miami, FL 33177- USA
phone: (305) 421-4952, fax: (305) 252-4407, email: hgraber@rsmas.miami.edu

William M. Drennan
Rosenstiel School of Marine and Atmospheric Science
University of Miami
4600 Rickenbacker Causeway
Miami, Florida 33149-1098
phone: (305) 421-4798, fax: (305) 421-4701, email: wdrennan@rsmas.miami.edu

Roland Romeiser
Rosenstiel School of Marine and Atmospheric Science
University of Miami
4600 Rickenbacker Causeway
Miami, Florida 33149-1098
phone: (305) 421-4645, fax: (305) 421-4701, email: rromeiser@miami.edu

Neil J. Williams
Rosenstiel School of Marine and Atmospheric Science
University of Miami
4600 Rickenbacker Causeway
Miami, Florida 33149-1098
phone: (305) 421-4656, fax: (305) 421-4701, email: nwilliams@rsmas.miami.edu

Michael J. Caruso
CSTARS - University of Miami
11811 SW 168th Street
Miami, FL 33177- USA
phone: (305) 421-4973, fax: (305) 252-4407, email: mcaruso@rsmas.miami.edu

Award #: N00014-09-1-0392

LONG-TERM GOALS

This proposal consists of six individual self-contained projects. A common component of all tasks is the exploitation of satellite imagery. The six projects are listed as the following tasks:

The long term goal of this project is to employ satellite SAR imagery to the quantitative analysis of typhoons, internal waves, ocean surface features, sea state prediction and coastal dynamics. To achieve this, a variety of satellite SAR sensors with different imaging frequencies, multi-polarizations and different beam modes are used to determine which combination of the above capabilities could provide the best solution.

OBJECTIVES

For simplicity we provide only a primary objective of each task.

a) Task 1: To determine the characteristics of typhoons with satellite SAR imagery and to measure with in-situ sensors the air-sea fluxes during the passage of typhoons.
b) Task 2: To complement the acquisition and analysis of conventional radar intensity images and other data by direct high-resolution imaging of surface current fields from space by along-track InSAR.
c) Task 3: To measure surface signatures and Bragg modulations during the passage of soliton packets.
d) Task 4: To improve the characterizations of the Philippine Archipelago Straits dynamics we propose to acquire satellite data, in particular synthetic aperture radar (SAR) imagery of features and processes present in these straits.
e) Task 5: To determine the structure, the seasonal and annual variability of the cold dome over the outer continental shelf northeast of Taiwan and the position and variability of the Kuroshio Current, in particular excursions onto the continental shelf.
f) Task 6: To explore innovative uses for commercial radar applications.

APPROACH

Task 1: From July to October 2010 a field experiment was carried out east of Taiwan in the primary region with high probability of typhoon tracks (Figure 1a). As part of the experiment we deployed two pairs of EASI (Extreme Air-Sea Interaction) and ASIS (Air-Sea Interaction Spar) buoys (Figure 1b) in international waters about 200 km apart. The buoys were equipped with extensive meteorological and oceanographic instrumentation to provide detailed measurements of the fluxes and properties of the air-sea interface.

We also utilized two remote sensing techniques which consisted of satellite-based imagery from RadarSat-2, TerraSar-X, Envisat ASAR, Cosmo-SkyMed and ERS-2; and a ship-borne marine X-band system (WaMoS) on the R/V Revelle. Figure 2 shows a summary of the quicklook images collected during Typhoon Megi. Using multiple satellite systems allowed for a good coverage of the storm after entering the experimental domain and across the Philippines and even into the Taiwan Straits. The synthetic aperture radar (SAR) images are especially valuable in determining the eye location and characteristics of storms. The radar backscatter data is used to derive wind speed and direction. Similarly the radar data can be used to estimate wave heights and wave directions. The marine radar systems on ships can also derive wind speed and direction, directional wave properties including

spectra from is grazing angle observations. The range of measurements from ship radar is more limited and extends to about 3 nm.

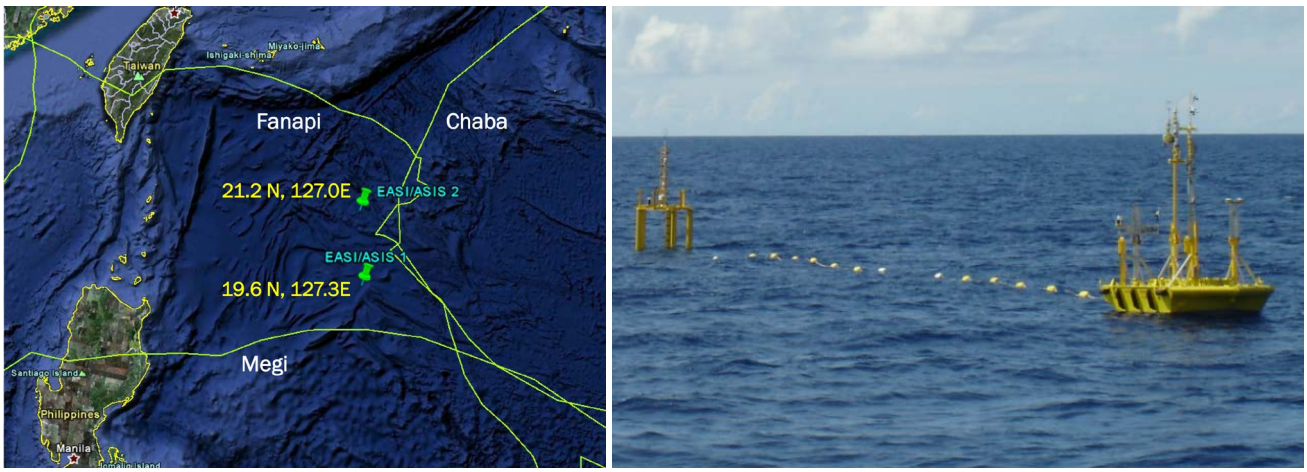

Figure 1: a) Deployment locations of the EASI/ASIS buoys in the Western Pacific with tracks of three of the typhoons passing by during the 2010 typhoon season. b) Deployed EASI/ASIS buoys in the Western Pacific.

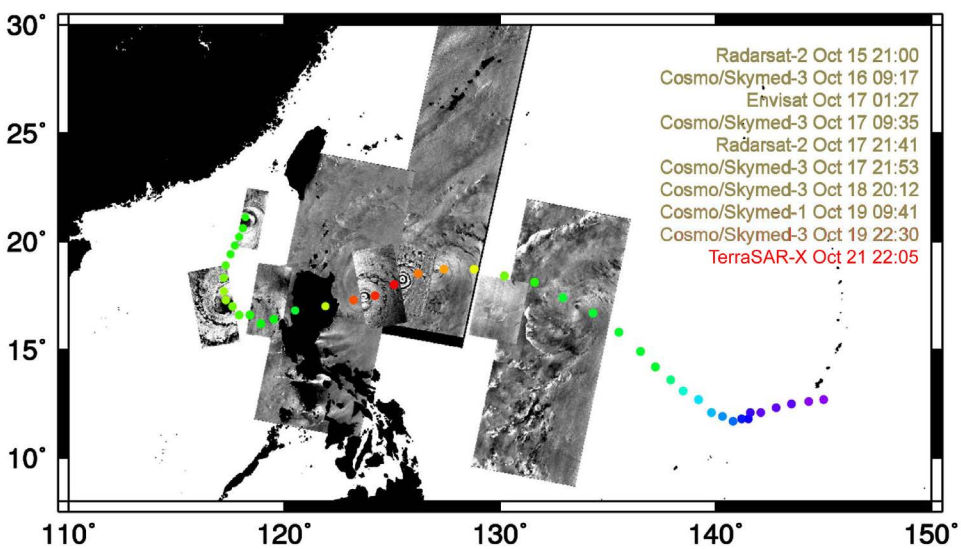

Figure 2: Multi satellite radar collections along the track of Typhoon Megi.

Task 5: In support of the main field program for the QPE DRI in August and September of 2009, we acquired 15 long strips of SAR images over the continental shelf northeast of Taiwan and the Kuroshio Current east of Taiwan. The collection focused on ascending and descending passes for ERS-2 and TerraSAR-X data using different beam modes that would include ScanSAR, standard and fine beam modes depending on the location. Similarly we collected MODIS SST images and other EO sensors that have infra-red channels such as ASTER (Advanced Spaceborne Thermal Emission and Reflection Radiometer), a high resolution imaging instrument flying on Terra.

Figure 3 shows a TerraSAR-X image over the northeast Taiwan shelf with abundant internal waves and soliton interaction patterns.

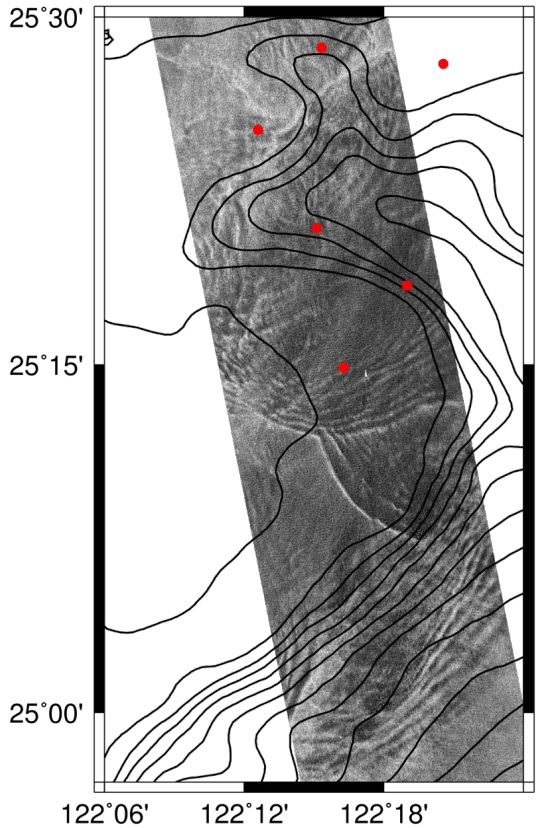

Figure 3: TerraSAR-X image collected on 9 August 2009 showing interacting internal wave patterns and soliton groups propagating in multiple directions.

WORK COMPLETED

Task 1: Data collection, both from satellite SARs and buoy measurements for the experimental phase of ITOP is completed. First results of SAR derived wind and wave fields of typhoons have been generated and made available to investigators. Extensive wind data set from shipborne marine X-band radar have been analyzed and a wind algorithm has been derived.

Task 2 and Task 3: Data analysis of both satellite and ship-based radar have been analyzed and new algorithms for classifying and characterizing internal waves are developed.

Task 4: This task is fully completed and a paper on gap jet winds has been published.

Task 5: Extensive satellite collections of EO and SAR sensors during the QPE experiment completed.

Data has been analyzed and shows some revealing characteristics of internal waves in this region.

Task 6: A new de-scalloping algorithm has been developed and can readily be applied as a post-processing procedure to ScanSAR images for TerraSAR-X, Cosmo-SkyMed and RadarSat-2 images.

RESULTS

Task 1: During the 2010 typhoon season the buoys encountered four major storms (Figure 1a), namely *Dianmu, Fanapi, Megi* and *Chaba*. The closest approach during these storms was around 100 km or in some cases less. While we hoped for closer approaches and the buoys were exposed to only moderate sustained winds in excess of 25 m/s and gusts reaching as much as 50 m/s, the generated waves attained significant wave heights of 10 m (Figure 4). Unfortunately both ASIS buoys broke loose as the surface tether failed due to fatigue from repeated slamming of the two buoys in intense sea state and wind conditions during the passage of super typhoons. ASIS North drifted and made a big loop eastward and then returned towards south and west where it was recovered near the southern mooring site. ASIS South was caught early after it broke loose.

Task 2 and 3: Marine radars operate by transmitting and receiving pulses of microwaves that interact with the rough sea surface. The radar echo from the sea surface is primarily dependent on small-scale ripple waves due to Bragg scattering. IWs are accompanied by a spatially and temporally varying surface current field. Marine radars show IWs as adjacent bands of weak and strong backscatter that propagate with the IW packet's velocity. As for SAR images, such features can either result from hydrodynamic interactions between the short surface waves and the horizontal surface currents caused by IWs, or from surfactants that accumulate in IW flow convergence zones and dampen the short surface waves there.

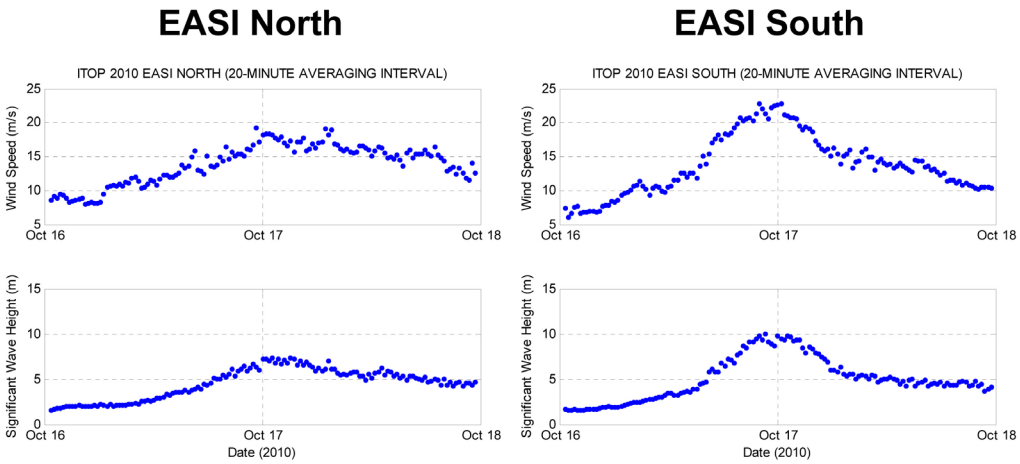

Figure 4: Wind speed and significant wave height measurements from EASI sites North and South during the passage of Typhoon Megi.

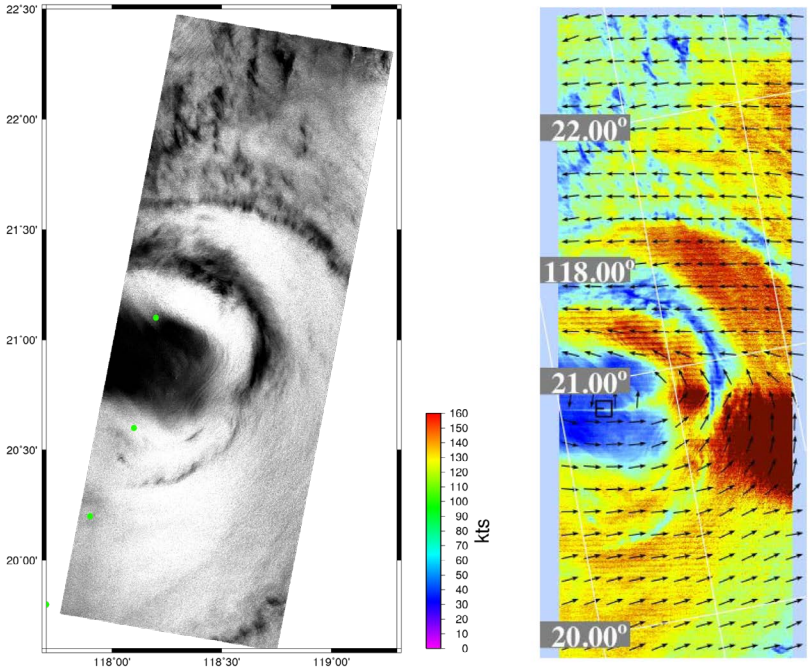

Figure 5: The original TerraSAR-X radar backscatter image at 18 m resolution taken on 21 October 2010 @ 22:05 UTC showing great detail of the eyewall of Megi (right) and SAR-derived wind vector field of Typhoon Megi (left) at 200 m spatial resolution.

SAR images have been used to demonstrate the existence of IWs in coastal oceans and derive IW parameters such as the propagation direction or the distance between solitons (see Task 5). More recently, methods to retrieve IW information from marine radar data have been introduced [R. J. Ramos, B. Lund, and H. C. Graber, 2009: "Determination of internal wave properties from x-band radar observations," *Ocean Eng.*, **36**(14), 1039–1047]. In contrast to SAR, where an IW packet is generally imaged only once, and in-situ measurements that provide "point" observations, marine radars provide a more complete picture as they allow to study the IW evolution.

We derived a novel method to retrieve IW information from marine radar data. First, the images are divided by their respective radar backscatter ramps to produce near-homogeneous intensities. The ramp-corrected images are then used to retrieve IW packet speed and direction, employing a combination of Radon transform and cross-correlation techniques. In a next step, the images are geo-referenced and corrected for the IW packet motion. By averaging a 4 min sequence of such preprocessed radar images, we can now significantly enhance the IW signatures. The resulting IW-enhanced images are fed into our IW signature retrieval algorithm, where we use localized Radon transform techniques to trace the signatures of each individual soliton, yielding IW soliton maps. From such maps, one can easily extract parameters such as wavelength, velocity, and curvature for each IW soliton.

Figure 6a shows the image transect from the IW-enhanced image with its IW peaks and troughs marked by black and red dashed lines, respectively. Finally, we use an iterative approach that is again based on localized Radon transform techniques to track each soliton, starting from the peaks found within the

transect. A zoom into our IW-enhanced image with the retrieved IW signatures as well as the position of the transect are shown in Figure 6b.

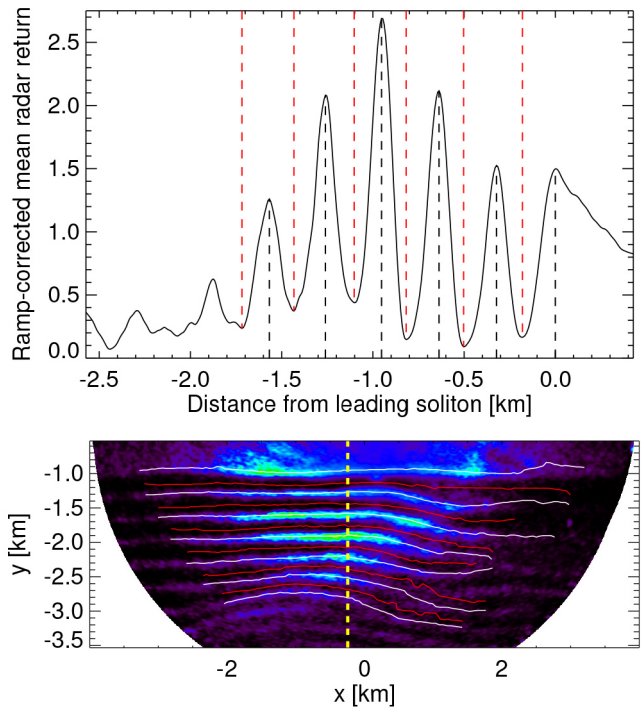

Figure 6: Transect with IW peaks and troughs marked by dashed lines (top) and corresponding image with the transect position marked by a yellow dashed line and the detected IW signatures marked by white and red solid lines (bottom).

Task 4: Gap jet characteristics were analyzed in the lee of the Philippine Archipelago during the 2004–2009 winter monsoon seasons (November–March) using wind fields derived from ENVISAT synthetic aperture radar (SAR) images. Jet characteristics were derived for the Philippine Island gap jets and compared to those from theoretical literature and experimental studies. It was found that 18 of 31 jets characterized from 13 SAR images followed the defined power laws, or classic case, and were similar to the defined scale equations. The remaining 13 jets did not follow the classic case and resulted from jet interaction with islands, adjacent jets, and variable atmospheric conditions. These non-classic jets were grouped based upon similarities and referred to as decreasing, increasing, and reverse classic cases. Distinct deviations from the classic case included downstream increases in velocity and decreases in jet width. It was found that the orientation of the wind field relative to topography significantly impacted jet classification, and thereby made it difficult to characterize jets by region. For all 31 jets, the initial jet width dictated the distance at which a jet became self-similar, wherein a larger initial jet width required a greater distance for self-similarity.

Figure 7 shows examples of gap jet wind fields derived from the SAR backscatter data. The jet features, long streaks emanating out of the valleys are quite obvious in contrast to the low wind speeds in the shadow (lee) of the mountain peaks.

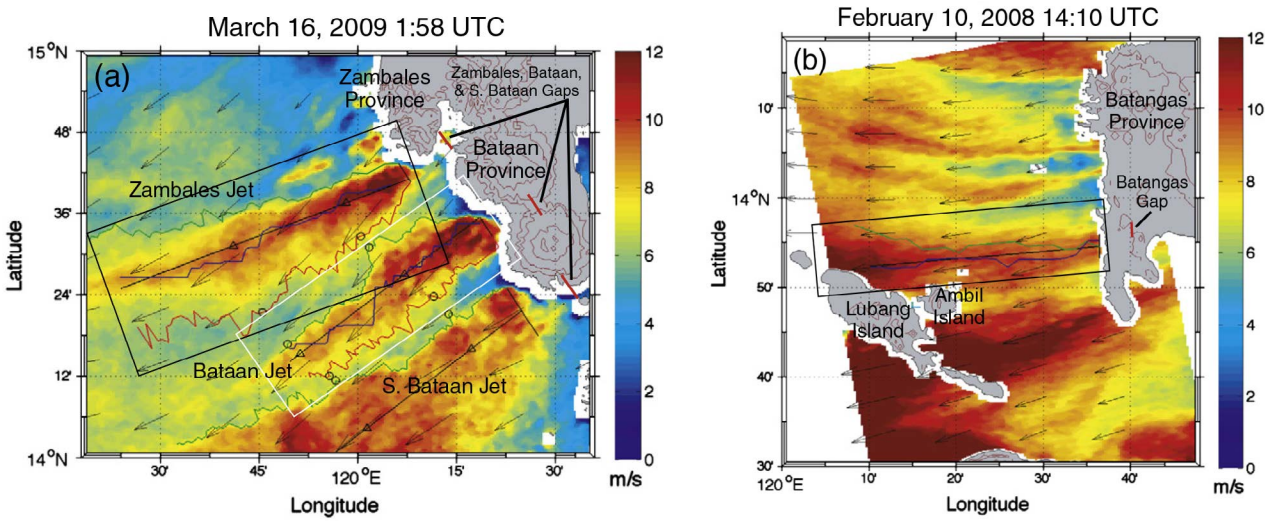

Figure 7: Examples of (a) classic (black box) and decreasing (white box) jet cases on March 16, 2009 1:58 UTC and (b) increasing jet case on February 10, 2008 14:10 UTC. The background is SAR-derived wind speed (m/s), with vectors denoting SAR-derived wind direction. Rectangular boxes denote the jets of interest. The green line denotes jet half-width (km), the perpendicular black line represents initial jet width (d, km), the straight black line is the jet centerline, and the blue line represents wind speed maxima (m/s) coordinates associated with the Principal Component Analysis technique from which the jet centerline is fit. Here d=6 km for (a) and d=5 for (b).

Task 5: The ocean northeast of Taiwan has a large continental shelf, complex slope bathymetry, an upwelling region, a variable coastal current, a strong boundary current and abundant internal waves. Intense fishing activity inhibits comprehensive mooring measurements. These features make it difficult to understand the physical processes of this region. Satellite synthetic aperture radar images were collected to the northeast of Taiwan as part of a focused field observation program during August and September 2009. Non-linear internal waves are observed in the satellite imagery and are used to deduce propagation patterns. The internal waves in this region are characterized by elaborate wave patterns created by multiple internal wave propagation directions and intersection angles. Although the images acquired show complicated internal wave patterns, three preferred pathways were found to exist. The first is offshore to the southeast toward deep water. The second is northwest toward the coast of China similar to internal wave patterns observed in other shelf regions. The third is orthogonal to the first two, propagating to the northeast along the shelf break. This third pathway produces the complex patterns frequently observed in satellite imagery of the region.

The majority of internal waves along the shelfbreak are classic depression waves generated by the internal tide along the shelfbreak. The remaining internal wave signatures are possibly generated by the encroachment of the Kuroshio Current on the shelf or the persistent cold dome. Additional internal waves may be trans-basin waves advecting onto the shelf from the Ilan Ridge or may be remnants of interacting wave packets (Figure 8). From the analysis of the imagery we found 220 internal wave (IW) packets with more than 2,407 waves (cf. Figure 8). There are clearly some hotspots of persistent internal waves located on the shelf and over the entrance to the canyons.

The histogram of propagation directions (Figure 9) shows the primary pathways are generally oriented perpendicular to the bathymetry. The majority of the internal wave packets are traveling southeast (90°

- 150°) toward the open ocean. The secondary propagation direction is to the northeast (270° - 330°) toward the coast. This propagation direction is frequently seen along the shelf in the South China Sea and the New York/Mid Atlantic Bight. A tertiary pathway exists towards the northeast (30° - 90°) along the shelf break. Note that the range of propagation directions along shore and offshore results in a peak in the histogram at the arbitrary delineation of 90° toward the east.

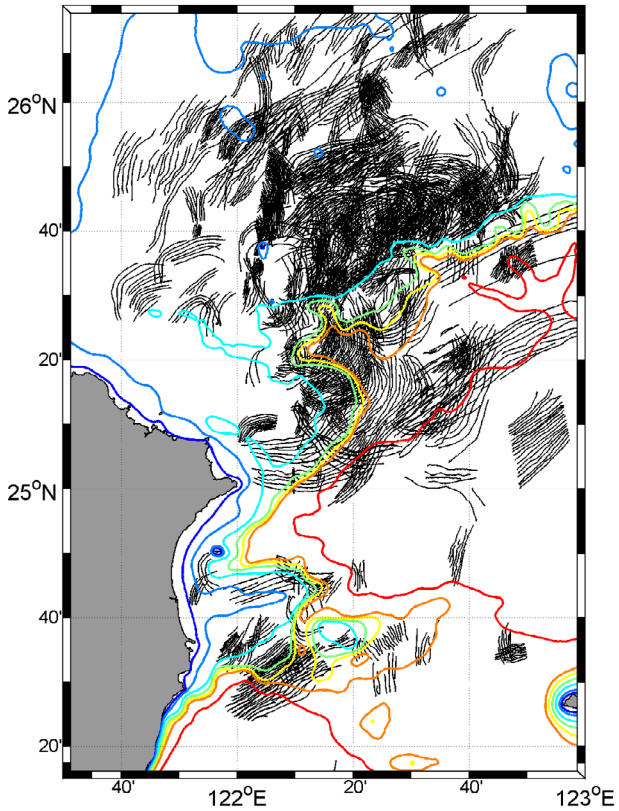

Figure 8: Locations of internal wave fronts identified from SAR imagery acquired between 2007 and 2010 from ERS-2 and TerraSAR-X.

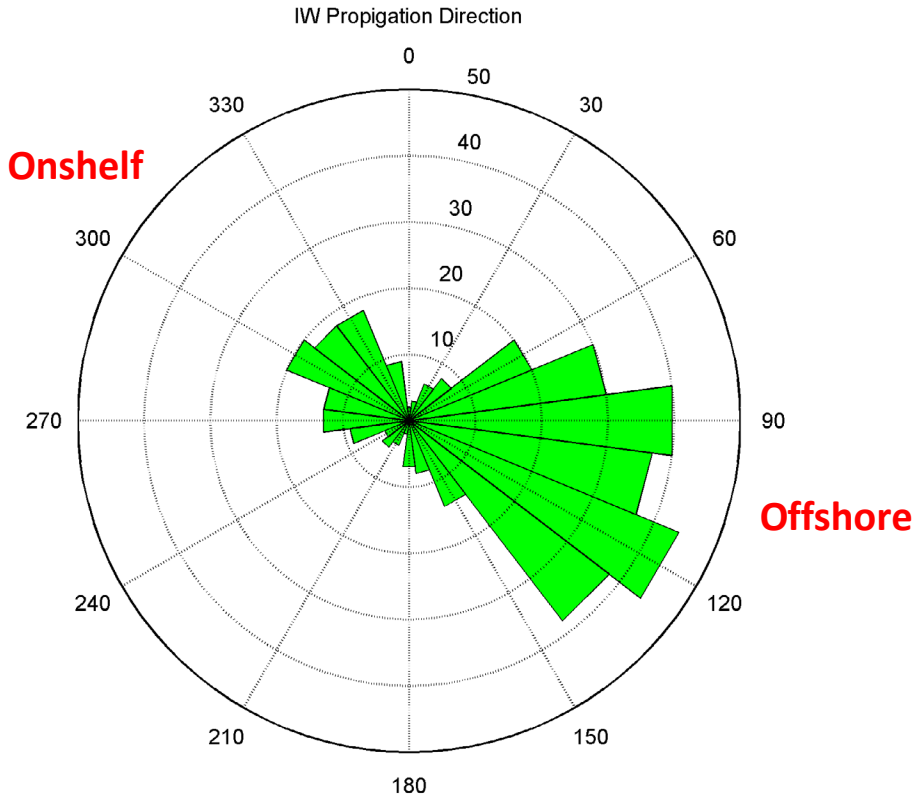

Figure 9: The propagation direction of internal waves from historical data. The northwest or onshore direction and southeast or offshore directions are dominant. However, internal waves also travel to the southwest toward the east coast of Taiwan. Internal waves also propagate toward the northeast along the shelfbreak.

IMPACT/APPLICATIONS

Space-based and ship-based radar remote sensing will provide new data and information on environmental parameters of the ocean such as ocean winds, storm winds, surface currents and internal waves.

TRANSITIONS

None.

PUBLICATIONS

Task 1:

Lund, B., **H.C. Graber**, R. Romeiser, 2012: Wind retrieval from shipborne nautical X-band radar data. *IEEE Trans. Geosci. Rem. Sens*., **50**(10), 3800 – 3811.

B. Lund, H.C. Graber, J. Horstmann, and E. Terrill, 2012: Ocean surface wind retrieval from stationary and moving platform marine radar data. *IGARSS 2012*, München, Germany, 22-27 July 2012.

Task 2 and 3:

Lund, B., **H.C. Graber**, J. Xue, and R. Romeiser, 2012: Analysis of internal wave signatures in marine radar data. *IEEE Trans. Geosci. Rem. Sens*. [in press].

Xue, J., **H.C. Graber**, B. Lund, and R. Romeiser, 2012: Amplitudes estimation of large internal solitary waves in the mid-atlantic bight using synthetic aperture radar and marine x-band radar images. *IEEE Trans. Geosci. Rem. Sens*. [in press].

B. Lund, J. Xue, R. Romeiser, and **H.C. Graber**, 2012: Retrieval of internal wave signatures from marine radar data. *IGARSS 2012*, München, Germany, 22-27 July 2012.

J. Xue, B. Lund, **H.C. Graber**, and R. Romeiser, 2012: A case study of internal wave-wave interaction patterns shown in the satellite images in the mid-atlantic bight. *IGARSS 2012*, München, Germany, 22-27 July 2012.

Task 4:

Gierach, M.M., **H.C. Graber**, M.J.Caruso, 2012: SAR-derived gap jet characteristics in the lee of the Philippine Archipelago. *Rem. Sens. Environ.,* **117**, 289-300. (doi:10.1016/j.rse.2011.10.004)

Task 5:

Duda, T.F., A.E. Newhall, G. Gawarkiewicz, M.J. Caruso, **H.C. Graber**, Y.-J. Yang, J. Sen, 2012: Significant internal waves and internal tides at a shelf edge and canyon region northeast of Taiwan. *J. Mar. Res.* (Special Issue), [in press].

Caruso, M.J., R. Ramos, **H.C. Graber**, 2012: Internal wave propagation pathways off northeast Taiwan. *J. Mar. Res.* (Special Issue), [in press].

Task 6:

Romeiser, R., J. Horstmann, and **H.C. Graber**, 2010: A new scalloping filter algorithm for ScanSAR images. IGARSS 2010, Honolulu, 25-30 July 2010.

Romeiser, R., J. Horstmann, M.J. Caruso, and **H.C. Graber**, 2012: A descalloping post-processor for ScanSAR images of ocean scenes. IEEE Trans. Geosci. Rem. Sens., [in press].